BNL-107608-2015-JA

Nanowire growth by an electron beam induced massive phase transformation

Shantanu Sood[1], Kim Kisslinger[2], Perena Gouma[1]

[1]State University of New York, Stony Brook, NY 11794-2275

[2]Brookhaven National Laboratory, Upton, NY 11973-5000

Abstract

Tungsten trioxide nanowires of a high aspect ratio have been synthesized in-situ in a TEM under an electron beam of current density 14A/cm^2 due to a massive polymorphic reaction. Sol-gel processed pseudocubic phase nanocrystals of tungsten trioxide were seen to rapidly transform to one dimensional monoclinic phase configurations, and this reaction was independent of the substrate on which the material was deposited. The mechanism of the self-catalyzed polymorphic transition and accompanying radical shape change is a typical characteristic of metastable to stable phase transformations in nanostructured polymorphic metal oxides. A heuristic model is used to confirm the metastable to stable growth mechanism. The findings are important to the control electron beam deposition of nanowires for functional applications starting from colloidal precursors.

Keywords: Nanowires; In-situ TEM; Sol-gel; one-dimentional nanostructures; tungsten trioxide

Introduction

Nanowires of semiconducting materials are nanostructures with high-aspect ratio, enormous surface area, and controlled crystallographic orientation that make them ideal for applications in sensing in a breath diagnostic tool[1], catalysis, and nano-electronics devices[2-3]. Such nanostructures have been widely considered in the literature since the early report of single crystal silicon by a vapor-liquid solid technique[4] and single crystal semiconducting nanowires have been synthesized by pulsed-laser ablation[6]. Monocrystalline nanowires of metal oxides (WO_3, MoO_3, CuO etc) have been produced

through various routes, from thermal oxidation of a metal mesh, to template-assisted blend electrospining, to colloidal synthesis of oxides[5-9]. WO_3 nanowires, in particular, have also been synthesized from growth directly from tungsten substrate[10] or by thermal heating of a tungsten plate[12]. Non-aqueous preparation of crystalline tungsten oxide nanowires has been carried out using a tungsten isopropoxide precursor in benzyl alcohol[12]. Nevertheless, there has been no direct observation of WO_3 nanowire growth in-situ and solely from solid oxide precursors until now, and thus the nature of the spontaneous transition of oxide nanocrystals to nanowires under the influence of an electron beam is being addressed here.

The focus of this article is the instantaneous growth of highly aligned nanowires of the monoclinic polymorph from metastable phase sol-gel nanoparticle precursors. The morphological transformation is a rapid manifestation of a self-catalytic phase reaction occurring in vacuum. The reaction appears to be self-catalyzed due to the instability of the metastable phase nanoparticles under the influence of the beam. It is shown that the nanoparticles due to the electron energy of the beam become wire-like growing into highly aligned periodic crystalline structures. This finding has important implications for achieving scalable and controlled nanowire synthesis.

Pseudocubic WO_3 precursor phase

The WO_3 nanoparticles were synthesized using a sol-gel route. Tungsten Isopropoxide (5% w/v in Isopropanol, Alfa Aesar) was used in equal quantities with, ethanol and acetic acid (to control pH) to synthesize the sol. The mixture was ultrasonicated and aged for 24 hours, upon which white precipitates were observed, indicating the completion of hydrolysis. The synthesized nanoparticles were subsequently dried in air and this resulted in a brownish powder. Finally the powder was heat-treated at 350^{o}C in a tube furnace for 8 hours resulting in a yellowish powder. This resulted is the formation of a metastable pseudocubic phase which has been observed earlier using similar synthesis technique[11].

Upon continuing the heat treatment, the particles were seen to transform to the stable orthorhombic phase between 500° and 550° Celsius.

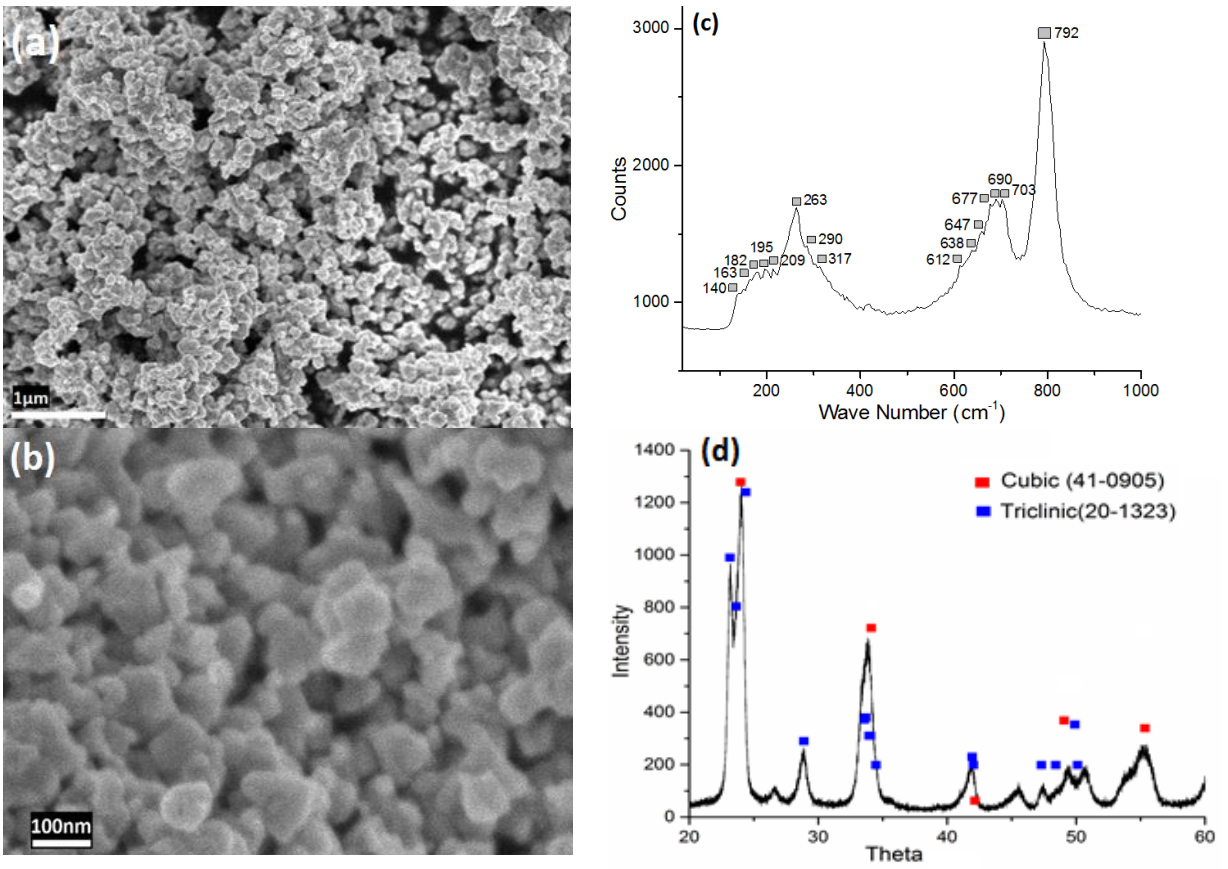

Figure 1: (a) Low magnification SEM image of sol-gel synthesized nanoparticles of tungsten trioxide annealed at 350C, **(b)** shows the higher magnification SEM image with uniformly distributed particle size. **(c)** Shows the Raman spectra of the nanoparticles, the bands observed are marked. **(d)** Shows the XRD of the nanoparticles.

SEM was done on a JEOL 7600F analytical high resolution SEM. The images in Figure 1 (a) and (b) show a uniform distribution of nanoparticles of radii 30-40nm. Crystalline size calculated from XRD using Scherrer equation gives a value of roughly 38.5nm. A preliminary analysis by looking at the nanoparticles points to the observation that there is no multiphase distribution. Figure 1 (c) shows the Raman spectra of the annealed nanoparticles. Raman studies were performed on a Witec Alpha combination near field optical and raman microscope. The W-O-W stretching mode that is the characteristic of the WO_6

octahedra can be observed at 792cm^{-1}, although with a slight shift. The peaks between 740cm^{-1} and 980cm^{-1} point to the presence of distorted octahedral[5]. The broad band observed in the spectra between starting about 150 to 400 can be ascribed to the cubic phase[24]. Similarly a broad instead of sharper peaks between 600cm^{-1} and 850cm^{-1} can also be ascribed to the cubic phase[24]. The triclinic phase shows peaks[25] between 240cm^{-1} and 270cm^{-1} in addition to one at 324cm^{-1}, although this is not sufficient to distinguish it from the monoclinic phase. Figure 1 (c) shows the XRD of the nanoparticles annealed at 350˚C. XRD was performed on a Rigaku Ultima III X-Ray diffractometer. All the peaks of the cubic phase, JCPDS card #41-0905, can be identified, although many peaks of triclinic phase can also be identified. This points to distortions in the crystal, which can also be confirmed by the SAD pattern shown in figure 2(Right) where we can observe the presence of other dimmer rings in addition to the rings corresponding to the (100); (110); (210) planes of the metastable cubic phase of tungsten trioxide. The nanoparticles of cubic tungsten trioxide are shown in figure 2(Left), were characterized under a JEOL JEM-1400 analytical TEM.

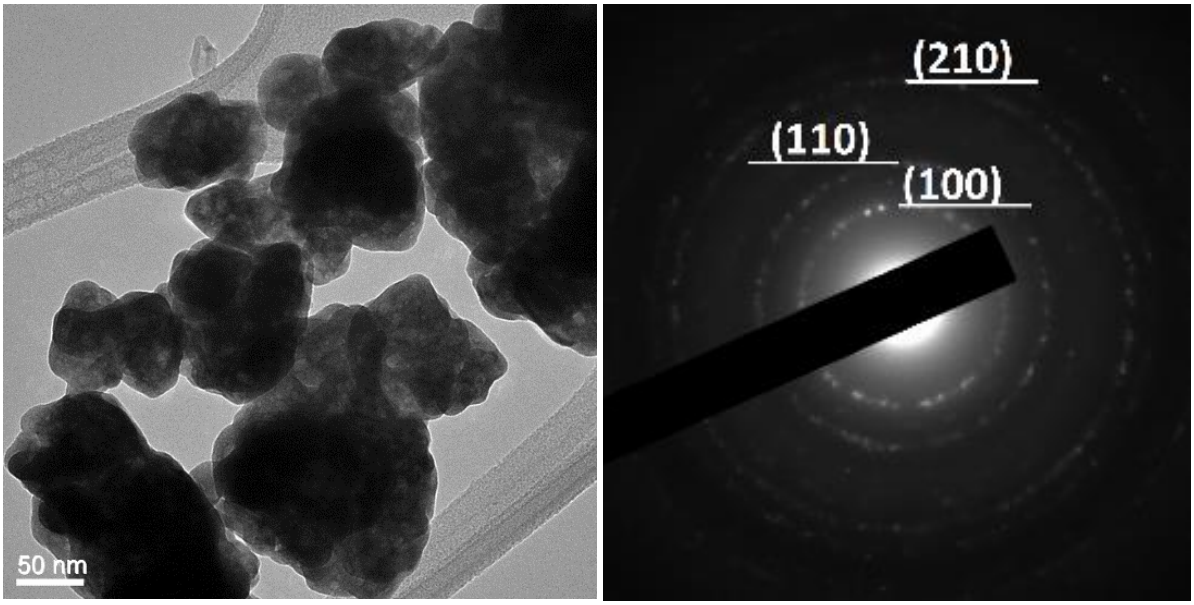

Figure 2 (Left): TEM micrograph of the cubic nanoparticles of Tungsten trioxide, **(Right)** SAD pattern, brighter rings can be indexed to (100); (110); (210) planes of the cubic phase.

Spontaneous growth of monoclinic WO_3 nanowires under electron beam irradiation

The prepared nanoparticles were drop coated onto a TEM grid consisting of a Formvar supporting film (200 Mesh Copper grids with support films, TED PELLA Inc.). Formvar is a family of polymers formed from polyvinyl alcohol and formaldehyde as copolymers with polyvinyl acetate[14], they are non-reactive class of compounds[16] and additionally have a NFPA 704 reactivity rating of 0. The formvar film was intact after the growth and EDS analysis (attached in the supplemental material, figure S1) showed no carbon on the nanowires (very small atomic percentages (small peak) is observed, which can be attributed to the presence of supporting film in the vicinity, similarly the copper peak is due to the copper mesh of the TEM grid). To completely rule out the possibility of the transformation being affected by the presence of carbon on the support film, the nanowire growth was carried on a grid containing Silicon Nitride as support film, the nanowires grew similar to the formvar support film. Figure 3 (Left) and (Right) images shows the SEM of nanowires grown on Silicon Nitride support film and TEM of nanowires grown on the Formvar support film.

Nanowires grown on Silicone Nitride support films Nanowires grown on Formvar support films

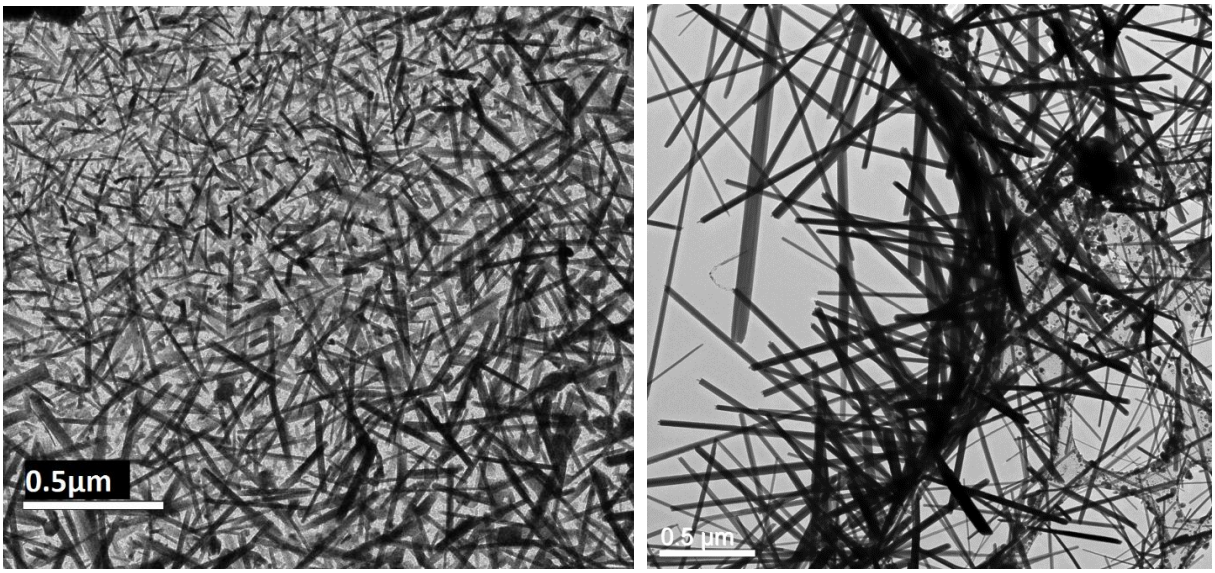

Figure 3: (Left) TEM of nanowires grown on a Silicon Nitride support film, **(Right)** TEM of nanowires grown on formvar support film on a Copper mesh grid.

A 120kV soft/bio materials analytical transmission electron microscope (JEOL JEM-1400) was used to grow the nanowires in-situ. The beam was spread initially while observing the nanoparticles and it was then slowly converged on the sample, the pseudocubic phase of the nanoparticles instantaneously grew into highly aligned nanowires (Figure 3) due to the energy imparted by the electron beam. Such an energy can be calculated. A 120keV electron beam was used for the nanowire growth. The JEOL JEM1400 TEM uses a LaB_6 filament as the electron source which gives a current density of 14A/cm^2 on the specimen when using a 0.8mrad illuminating aperture[17]. This current density can be converted to energy density using the power formula of current times voltage, which gives a value of 1680 joules/cm^2 for 1 second at 120kV accelerating voltage. For 5000X magnification, a focused electron beam of 120kV would provide 76keV of energy at the surface of an average 40nm grain size nanoparticle for about half a microsecond to instantly transform it to a monoclinic phase nanowire.

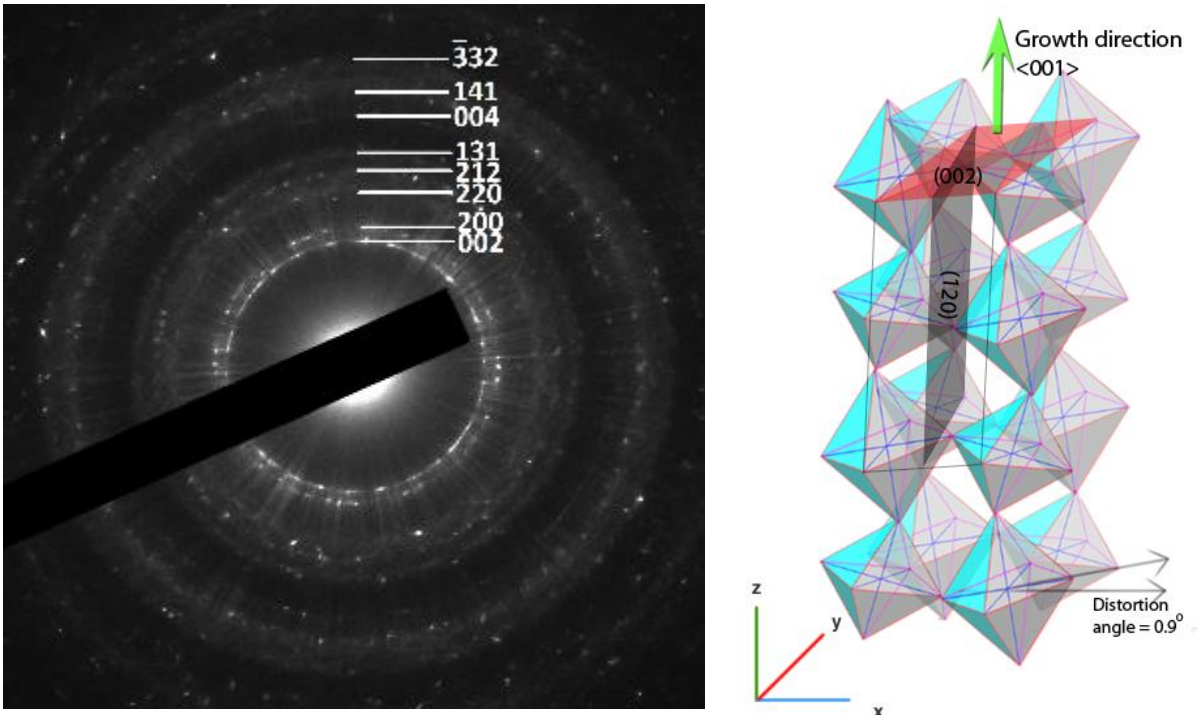

Figure 4: (Left) Typical Electron diffraction pattern taken from a region with high concentration of nanowires. (Right) Schematic of crystal structure of the monoclinic phase, with the preferred growth direction, the distortions have been exaggerated to serve the purpose of illustration.

The high concentration of nanowires causes a distinct diffraction pattern at high magnification, the diffraction pattern can be made into a ring pattern by reducing the magnification and taking a larger sample area into focus, figure 4(left). The rings correspond to lattice planes (002), (200), (220), (212), (131), (004), (141), ($\bar{3}$32), in Figure 4(left), of the monoclinic γ-WO_3 (JCPDS #43-1035). A ReO_3 type corner sharing octahedral forms the basic building block of all phases of tungsten trioxide. The crystal lattice symmetry of monoclinic WO_3 is a distorted rhenium oxide cubic configuration, figure 4(Right).

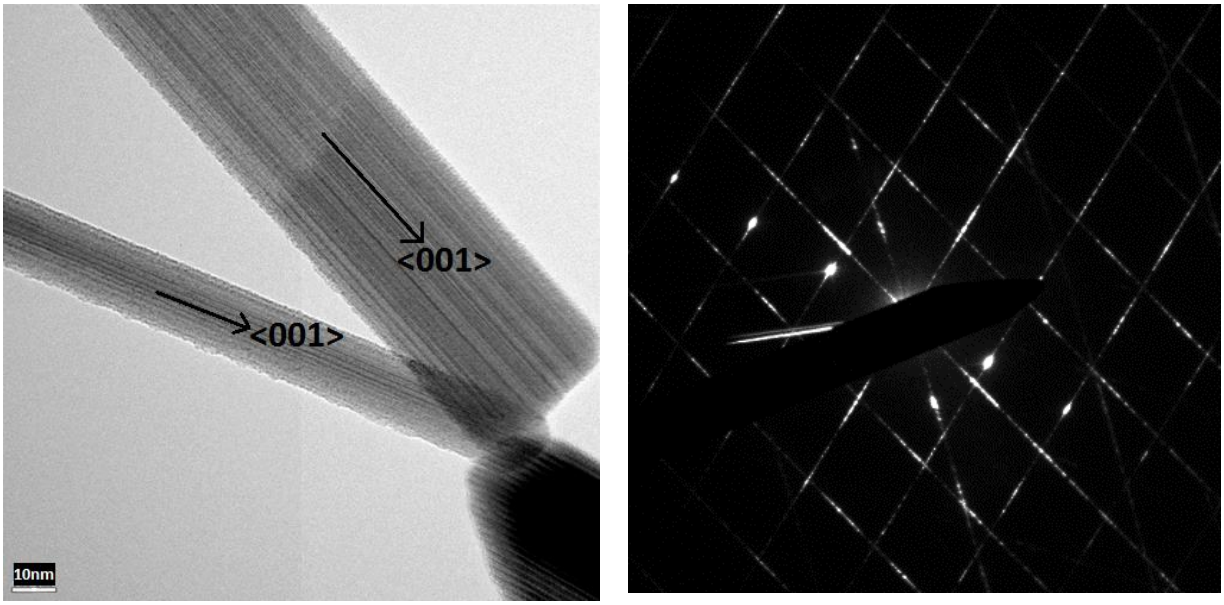

Figure 5: (Left) Highly aligned nanowires, showing the <001> growth direction along the long axis; **(Right)** Corresponding diffraction pattern.

The nanowires grow in to highly aligned crystals, figure 5(Left) along the <001> direction, with the corresponding SAD pattern is shown in figure 5(Right). The high resolution TEM was carried out on JEOL 2100F Field Emission Lorentz TEM. The micrograph in figure 6 along with the SAD pattern in figure 6(Inset) gives a more detailed picture of the crystal structure. The spacing of 0.383nm and 0.33nm correspond to the (002) and (120) planes of the monoclinic phase of tungsten trioxide (JCPDS #43-1035). Growth direction of <001> perpendicular to the (002) plane is along the long axis of the nanowires.

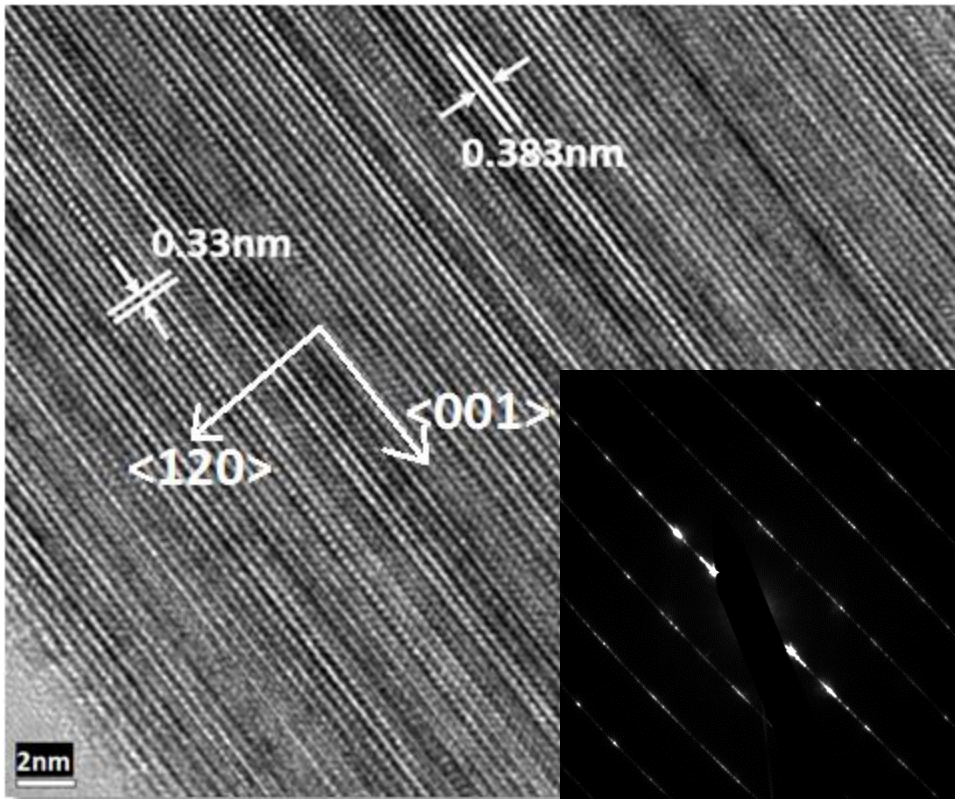

Figure 6: High resolution TEM of the structure of the nanowires; **(Inset)** SAD pattern from individual nanowire.

Mechanism for growth

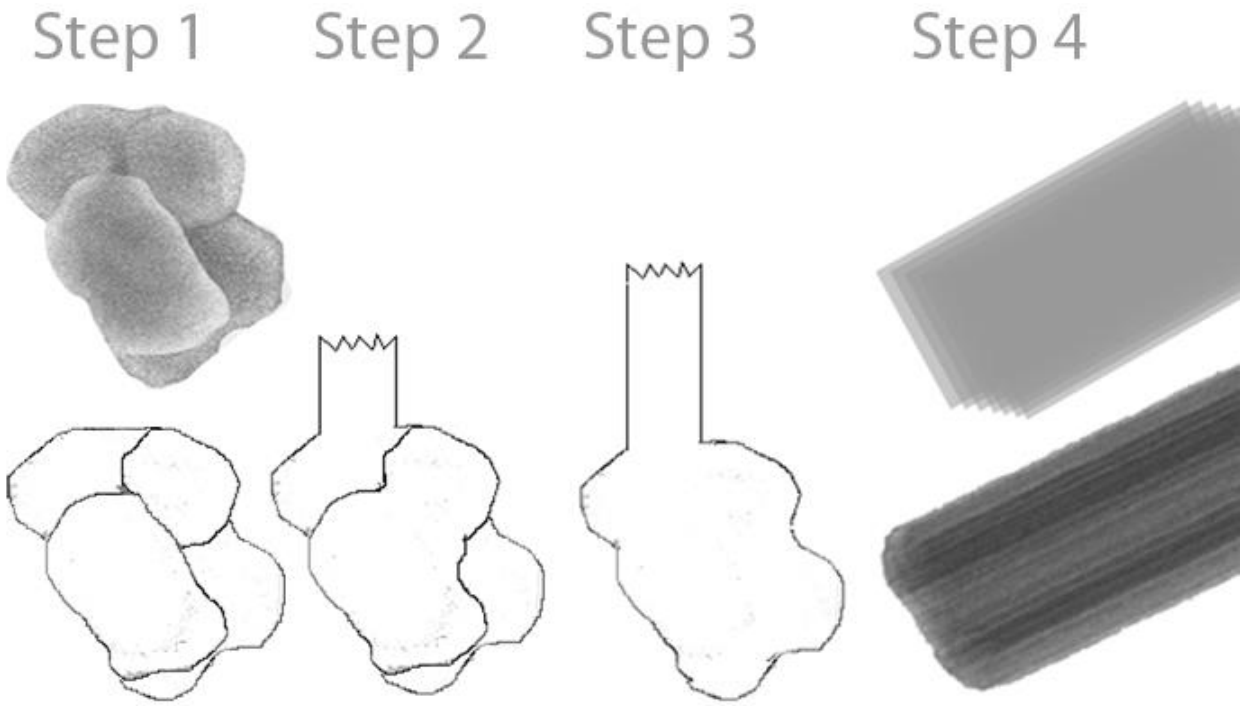

Figure 7: Schematic describing the growth of monoclinic tungsten trioxide nanowires from nanoparticles of pseudocubic phase in a stepwise fashion. Step 1 shows the starting nanoparticles which have a radius of between 30 to 40nm. As an electron beam is shown onto these nanoparticles the particles start to grow into nanowires as shown in step 2. As the nanoparticles get consumed they start to coagulate and grow into nanowires. Step 3 shows how these nanoparticles grow from preferred direction to form randomly oriented nanowires before being totally consumed and forming highly aligned nanowires of tungsten trioxide as shown in step 4. The whole process may take a few micro seconds to complete once the nanoparticles receive the required amount of energy.

It is interesting to note that an apparent transition from a metastable (pseudocubic) to a stable (monoclinic) polymorph has driven the nanowire growth. The DSC data (Figure S2 in supplemental material) which shows no weight loss for the heat treated sol-gel sample further supports this claim, and this is also apparent by comparing the DSC data of the before heat treatment (Figure S3 in supplemental material) and after heat treatment (Figure S2 in supplemental material). The data also supports the absence of any hydroxyl groups or interfering carbon impurities in the starting material. The mechanism of massive nucleation and growth above a critical particle size of metastable phase has been previously established[18]. Experimentally such transformations have been observed in titania by Gouma et al.[19-20] as did the nanowire formation observed for the orthorhombic phase of MoO_3[8] system. Earlier work has also produced monocrystalline WO_3 nanowires[21]. The nucleation and growth of the stable phase can either occur randomly throughout the crystal by doing so at specific defects or crystal edges or such a growth can occur in a diffusive manner like a front moving forward at a fast rate. In the growth of nanowires in this study, it appears that phase change occurs rapidly by a moving front that results in a massive grain growth and radical shape change. The metastable phase particles on the path of the moving front are consumed and transformed, as shown in figure 7. As the nanowire growth proceeds the nanoparticles coalesce and get consumed which this gives rise to very long thin nanowires. The formed nanowires are one-dimensional structures which potentially grow as this front rapidly grows out of the pseudocubic phase into the preferred <001> monoclinic direction. The rel-rod type diffraction

pattern observed, figure 5(Right) and figure 6(Inset) lend credibility to this argument[22]. A cubic to monoclinic phase transition has been previously observed in nanoparticles of ReO3 which is an isostructural material to WO_3[29]. A very large volume change is associated with such a transition which is analogous to the change observed in this study. Considering an average particle size of 40nm cubic phase, and an average 20nm radii and half a micron length nanowire, there is a 1000 fold increase in the volume during this transition. Additionally a lowering of external perturbation required (pressure in that case) was also reported to be much lower than that required for the bulk ReO_3. There has been no direct observation of cubic to monoclinic phase transformation in tungsten trioxide nanocrystals, which maybe due to the high energies involved in the transformation in the bulk phase. Although a cubic to orthorhombic phase transformation has been observed[23], as both orthorhombic and monoclinic phase of tungsten trioxide are stable polymorphic structures.

Thermodynamic mechanism for metastable to stable phase transition

By exploring the theoretical mechanism which governs the metastable to stable phase transitions in nanocrystalline materials[18] we can further explain the growth of stable phase nanowires. The thermodynamic data for a psuedocubic phase was unavailable, thus that of cubic is used. The free energy of a nanoparticles system ($\Delta G^{NS}(T,r)$) or a nanowire system ($\Delta G^{NW}(T,r)$) depends on three factors, surface free energy ($\Delta G_S(T,r)$), surface stress ($\Delta G_P(T,r)$), and free energy due to particle shape ($\Delta G_G(T,r)$), as discussed in previously published work by the authors[18]. Thus,

$$\Delta G^{NS}(T,r) = \Delta G^{\infty}(T,r) + \Delta G_S(T,r) + \Delta G_P(T,r) + \Delta G_G(T,r) \quad (1)$$

$$\Delta G^{NS}(T,r) = A_m.\gamma + P_{in}.V + \alpha.\Delta^{\infty}H_f.(A/V) \quad (2)$$

Where, γ is the surface energy/tension which is different from f_s which is the surface stress, A_m is the molar area, P_{in} is the internal pressure, V is the molar volume, α is a shape constant and $\Delta^{\infty}H_f$ is the enthalpy of formation of the bulk phase.

Table 1: Contributions from the three main factors influencing the nanowire growth.

	Nanoparticle/Nanosphere	**Nanowire/Nanocylinder**
$\Delta G_S(T,r)$	$(4.\pi.r^2).\gamma$	$(2.\pi.r^2 + 2.\pi.r.h).\gamma$ [Appendix A]
$\Delta G_P(T,r)$	$(2.f_s/r).\ (4.\pi.r^3/3)$	$[(1/h + 1/\pi.r).2.f_s].(\pi.r^2.h)$
$\Delta G_G(T,r)$	$\alpha.\Delta^{\infty}H_f/2.r$	$\alpha.\Delta^{\infty}H_f.(2/h + 2/r)$ [Appendix B]

Therefore, the free energy for the nanowire ($\Delta G^{NW}(T,r)$) and nanoparticles ($\Delta G^{NS}(T,r)$), systems can be given by,

$$\Delta G^{NS}(T,r) = (4.\pi.r^2).\gamma + (2.f_s/r).\ (4.\pi.r^3/3) + \alpha.\Delta_S^{\infty}H_f/2.r \quad (3)$$

$$\Delta G^{NW}(T,r) = (2.\pi.r^2 + 2.\pi.r.h).\gamma + [(1/h + 1/\pi.r).2.f_s].(\pi.r^2.h) + \alpha.\Delta_C^{\infty}H_f.(2/h + 2/r) \quad (4)$$

Table 2: Data accumulated from the literature, and the free energy calculations

Observed Nanowire radius	20nm
Predicted Nanowire length	560nm
Average nanoparticle radius	40nm
$\gamma_{monoclinic}$	0.625 J/m^2 [26]
γ_{cubic}	1.67 J/m^2 for (001) plane[26]
$\Delta^{\infty}H_{f\ (cubic)}$	- 6.69 X 10^{-13} J [27]; (Appendix C)
$\Delta^{\infty}H_{f\ (monoclinic)}$	-2.67 * 10^{-13} J (Appendix C)
$f_{s(monoclinic)}$	2.5 J/m^2($2.\gamma_m$)
$f_{s(cubic)}$	3.34 J/m^2 ($2.\ \gamma_c$)

α	2nm[28]
$\Delta G^{NS}(T,r)$	384.04 KeV
$\Delta G^{NW}(T,r)$	456.709 KeV

Table 2 tabulates all the values substituted and the results for the free energy. It can be seen that the free energy values for nanowires is greater than for nanoparticles. Thus for the transformation to occur an external source with the energy equivalent to the difference in the free energy of nanowire and nanoparticle is necessary for the growth to occur. $\Delta G^{NW}(T,r) - \Delta G^{NS}(T,r) = 72.671$ KeV. Thus from equation, $\Delta E = 72.671$ KeV, which is in range of the energy provided (76keV) by the electron beam at the surface of an average size nanoparticle.

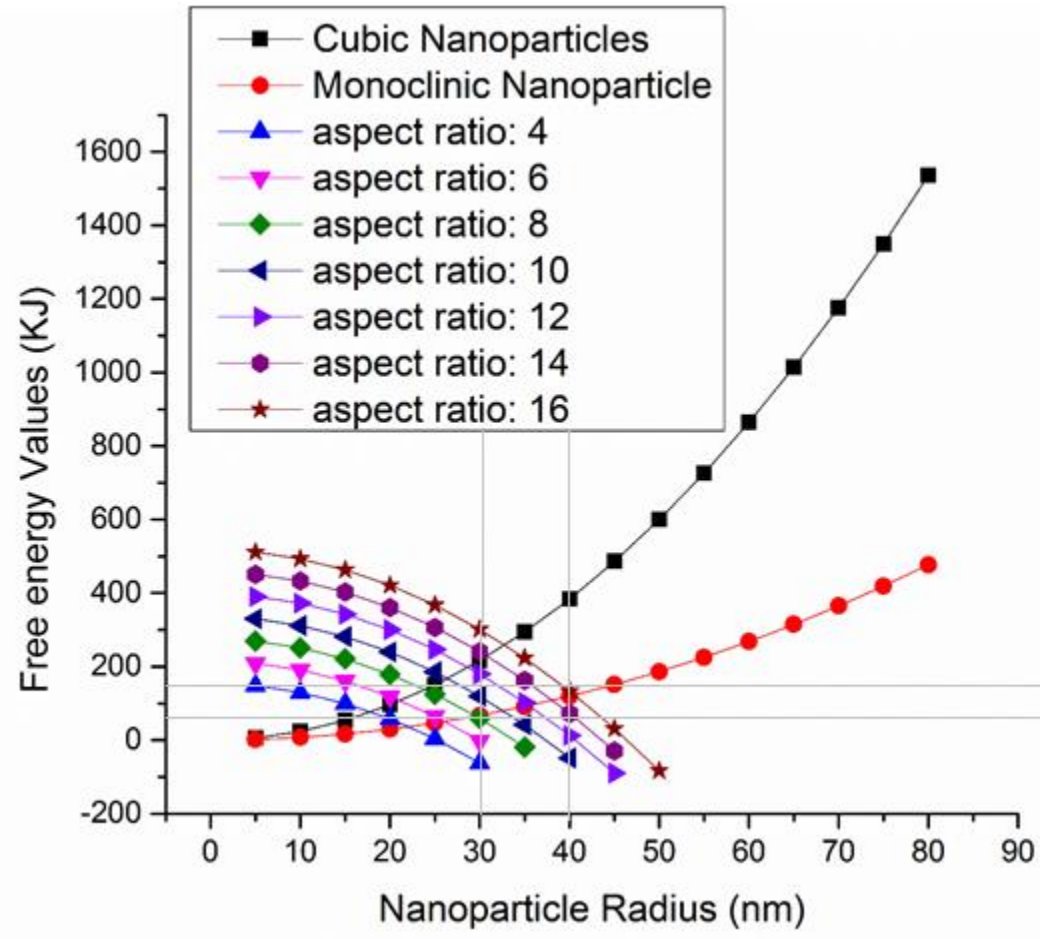

Figure 8: Graph plotting the free energy for cubic and monoclinic phase due to particle size, and overlay is the difference in the free energies for cubic nanoparticles and monoclinic nanowires as a function of the aspect ratio of the nanowires keeping the radius of nanowires constant at the observed values 20nm.

Figure 8, plots two overlaying graphs which give two different conclusion, first, the free energies inherent for cubic phase is plotted as a function of its particle radii, we may conclude that as the graph goes asymptotic for the particle size higher than 100nm, the cubic phase should be a metastable bulk phase which this is consistent. The monoclinic phase is more stable as the free energies are lower for higher particle size. Secondly, the $\Delta G^{NW}(T,r)$ - $\Delta G^{NS}(T,r)$ values for differing nanoparticle radius and the observed average nanowire radius of 20nm for varying aspect ratio is plotted, we earlier showed that the particle size distribution, figure 1(a, b) for precursor phase was between 30nm to 40nm, and the fact that there starts to be significant deviation in the free energies of nanoparticles of cubic and monoclinic phases at these particle sizes, this is consistent with the observations. We may conclude from this overlaying plot that the area of the graph between the free energy value of 80 to 120kv and the nanoparticle size of 30 to 40nm which gives us the expected aspect ratios of the nanowires which is from 12 to 16, is consistent with observed values of nanowire length (480nm to 640nm), figure 3.

We have demonstrated for the first time that tungsten trioxide nanowires of monoclinic phase can be grown as an apparent self-catalyzed reaction without any chemical reaction. The presence of metastable phase and a sufficiently large external perturbation is enough to drive the polymorphic reaction and shape change to nanowires on an inert surface in high vacuum conditions.

Appendix A: Internal pressure calculations

For the internal pressure calculations for cylindrical surfaces, the spherical liquid droplet should be replaced with a cylindrical surface.

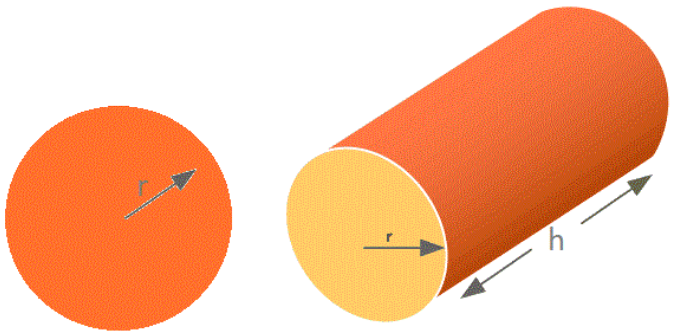

Figure 9: A liquid droplet with radius 'r', a hypothetical cylindrical droplet with radius 'r' and height 'h'.

Instead of a half sphere, we have a half cylinder as the droplet, thus, modifying laplace-young equation,

$$\Delta P_{in}.A = (\text{edge length}).(\text{surface tension}) \quad (5)$$

$$\Delta P_{in}(\pi.r.h)/2 = (\pi r + h).f_s \quad (6)$$

$$\Delta P_{in} = (1/h + 1/\pi.r).2.f_s \quad (7)$$

Appendix B: Free energy due to particle shape calculations

Due to lack of literature data on the value of α, we will consider it similar for both cylindrical and spherical particles, but the 1/r term which stems from the Area/Volume term is altered for considering the cylindrical shape of the nanowires. Thus, for cylindrical particle shape.

$$\Delta G_G(T,r) = \alpha.\Delta^{\infty}H_f.(A/V) = \alpha.\Delta^{\infty}H_f.(2/h + 2/r) \quad (8)$$

Appendix C: Number of molecules in average particle and enthalpy of formation calculations

The volume of single unit cell of cubic tungsten trioxide, can be calculated using the lattice constants given in the JCPDS file #41-0905, which comes out to be 5.12×10^{-29} m^3. Number of molecules in an average spherical particle of 40nm radius is given by,

$$\text{Volume of spherical particle/volume of single unit cell} = 5.23 \times 10^{6} \quad (9)$$

$$\Delta_S{}^{\infty}H_{f\,(cubic)} = -77.2\ KJ/mol^{27} = -6.69 \times 10^{-13}\ J / 5.23 \times 10^{6}\ particles \quad (10)$$

Similarly, the volume of single unit cell of monoclinc tungsten trioxide, can be calculated using the lattice constants given in the JCPDS file #43-1035, which comes out to be $2.11 \times 10^{-28}\ m^3$. Number of molecules in an average cylindrical particle of 20nm radius and 560nm length is given by,

$$\text{Volume of cylindrical particle/volume of single unit cell} = 3.33 \times 10^{6} \quad (11)$$

$$\Delta_S{}^{\infty}H_{f\,(monoclinic)} = -192.65\ KJ/mol = -2.67 * 10^{-13}\ J / 3.33*10^{6}\ particles \quad (12)$$

Acknowledgement

This research was funded by the NSF-IIS, grant #1231761. Research carried out (in part) at the Center for Functional Nanomaterials, Brookhaven National Laboratory, which is supported by the U.S. Department of Energy, Office of Basic Energy Sciences, under Contract No. DE-AC02-98CH10886.

References

1. P. Gouma, S. Sood (2013) 3-sensor Array for Hand Held Breath Diagnostic Tool. *MRS Online Proc. Lib.* 1533.
2. P. Gouma (2009). *Nanomaterials for Chemical Sensors and Biotechnology* (*Pan Stanford Publishing*.
3. L. Wang, P. Gouma (2012). *Integrated Microanalytical Systems*, chapter 5 (eds. M. A. Carpenter et al.), 167-188.
4. R.S. Wagner, W.C. Ellis (1964). Vapor-liquid-solid mechanism of single crystal growth. *Appl. Phys. Lett.* 4, 89.

5. G. L. Frey, Rothschild, J. Sloan, Rosentsveig, R. Popovitz Biro and R. Tenne (2001). Investigations of nonstoichiometric tungsten trioxide nanoparticles. *J. Solid State Chem.* 162, 300.
6. Y.F. Zhang, Y.H. Zhang, N. Wang, D.P. Yu, C.S. Lee, I. Bello, S.T. Lee (1998). Silicon nanowires prepared by laser ablation at high temperatures. *Appl. Phys. Lett.* 72, 1835.
7. K. Sawicka, M. Karadge, P. I. Gouma (2004). Oxidation synthesized CuO nanowires for gas sensing applications. *Microsc. Microanal*. 10, 360-361.
8. P. Gouma, K. Kalyanasundaram, A. Bishop (2006). Electrospun Single Crystal MoO3 Nanowires for Bio-Chem sensing probes *J. Mat. Res.* 21(11), 2904-2910.
9. Patent granted US/Patent No 7,981,215 issued on 07/19/2011, entitled "Electrospun Single Crystal MoO3 Nanowires for Bio-Chem Sensing Probes"
10. Fusheng Xu, Stephen D. Tse, Jafar F. Al-Sharab and Bernard H. Kear (2006). Flame synthesis of aligned tungsten oxide nanowires. *Appl. Phys. Lett.* 88, 243115.
11. A.K. Srivastava, S.A. Agnihotry, M. Deepa (2006). Sol–gel derived tungsten oxide films with pseudocubic triclinic nanorods and nanoparticles. Thin Solid Films 515 1419–1423.
12. G.Y. Chen, V. Stolojan, D.C. Cox, C. Giusca, S.R.P. Silva (2006). Growth of tungsten oxide nanowires using simple thermal heating. *Emerging Technologies - Nanoelectronics,* IEEE Conference, 376.
13. Julien Polleux, Alexander Gurlo, Nicolae Barsan, Udo Weimar, Markus Antonietti, Markus Niederberger (2006). Template-Free Synthesis and Assembly of Single-Crystalline Tungsten Oxide Nanowires and their Gas-Sensing Properties. *Angew. Chem*. 118, 267-271.

14. E. Davison, W. Colquhoun (1985). Ultrathin formvar support films for transmission electron microscopy *J. Elect. Micros. Tech*. **2,** 35-43.
15. R. Diehl, G. Brandt (1978). The crystal structure of triclinic WO_3. *Acta Crystallogr. B* 34, 1105.
16. M. Stadermann, S. O. Kucheyev, J. Lewicki, and S. A. Letts(2012). Radiation tolerance of ultra-thin Formvar films. *Appl. Phys. Lett*. 101, 071908.
17. J. C. H. Spence (1981), *Experimental High-resolution Electron Microscopy* (Oxford Science Publications, pp250.
18. S. Sood, P. Gouma (2013). Polymorphic phase transitions in nanocrystalline binary metal oxides *J. Am. Ceram. Soc.,* 96 [2], 351–354.
19. P.I. Gouma, M.J. Mills (2001). Anatase to Rutile Transformation in Titania Powders *J. Am. Ceram. Soc*. 84(3), 619.
20. P.I. Gouma, P.K. Dutta, and M.J. Mills (1999). Structural Stability of Titania Thin Films *Nanostruct. Mater*. 11(8), 1231.
21. K.M. Sawicka, A.K. Prasad, P.I. Gouma (2005). Metal Oxide Nanowires for Use in Chemical Sensing Applications. *Sensor Letters* 3, 1-5.
22. A Baronnet, ZC Kang (1989). *Phase Transitions: A Multinational Journal* (Taylor & Francis).
23. Cs. Balazsi, M. Farkas-Jahnke, I. Kotsis, L. Petras, J. Pfeifer (2001). The observation of cubic tungsten trioxide at high temperature dehydration of tungstic acid hydrate. *Solid State Ionics* 141–142, 411–416.

24. L. Sangaletti, L. E. Depero, G. Sberveglieri, B. Alieri, E. Bontempi and S. Groppelli (1999). Growth of WO_3 crystals from W-Ti-O thin films. *J. Cryst. Gro.* 198/199, 1240.
25. E. Cazzanelli, C. Vinegoni, G. Mariotto, A. Kuzmin, and J. Purans (1999). Low-Temperature Polymorphism in Tungsten Trioxide Powders and Its Dependence on Mechanical Treatments. *J. Sol. St. Chem*. 143, 24D32.
26. Peter M. Oliver, Stephen C. Parker, Russell G. Egdell and Frances H. Jones (1996). Computer simulation of the surface structures of WO_3. *J. Chem. Soc., Faraday Trans.* 92(12), 2049-2056.
27. Furio Cora, Atul Patel, Nicholas M. Harrison, Roberto Dovesi and C. Richard A. Catlow (1996). An ab Initio Hartree-Fock Study of the Cubic and Tetragonal Phases of Bulk Tungsten Trioxide. *J. Am. Chem. Soc.* 118, 12174-1218
28. M. Wautelet (2000). Estimation of the Variation of the Melting Temperature with the size of Small Particles, on the Basis of a Surface-Phonon Instability model. *J. Phys. D: Appl. Phys*. 24, 343.
29. Kanishka Biswas, D V S Muthu, A K Sood, M B Kruger, B Chen and C N R Rao (2007). Pressure-induced phase transitions in nanocrystalline ReO_3. *J. Phys.: Condens. Matter* **19**, 436214

Supplementary information

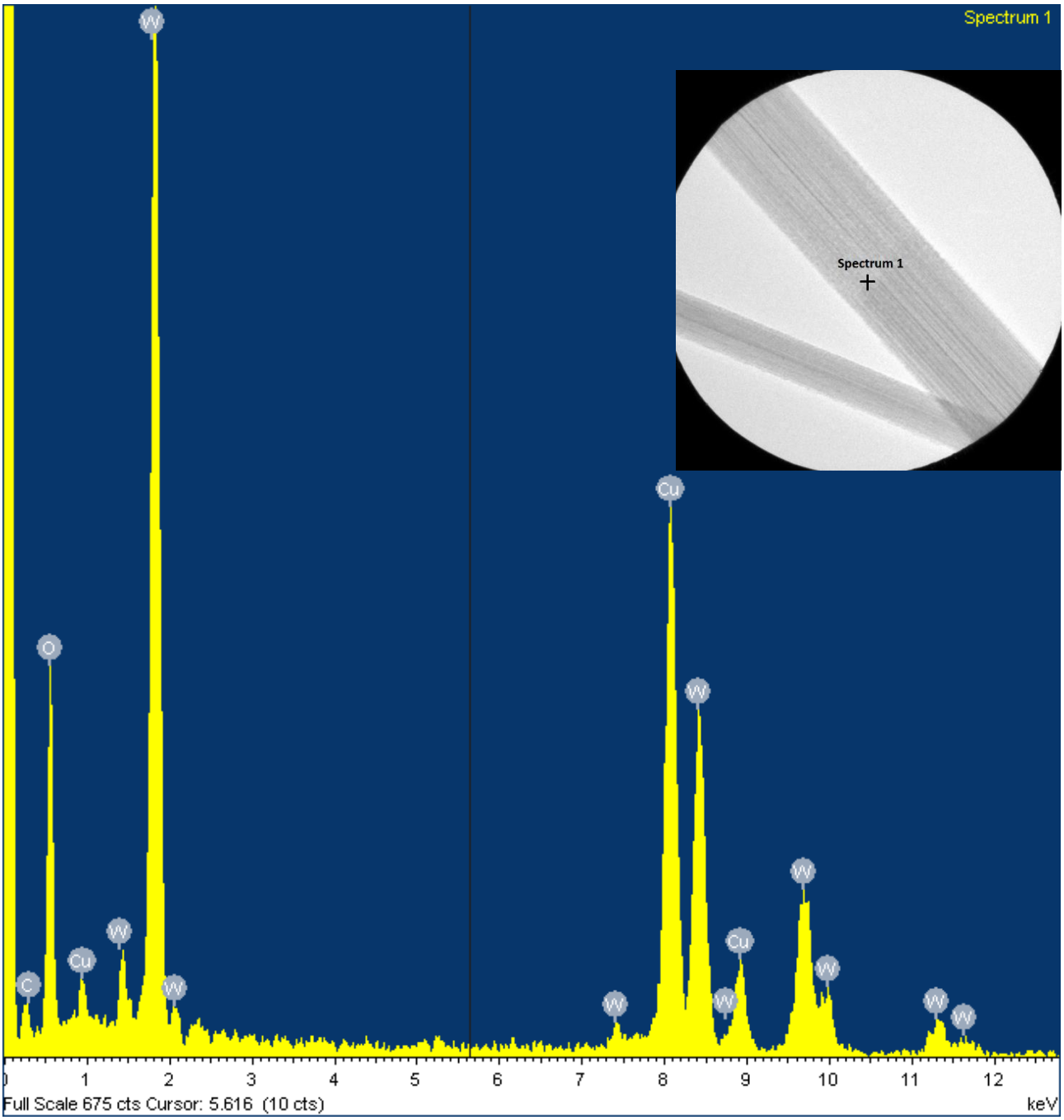

Figure S1: EDS spectra from the nanowires showing the presence of tungsten and oxygen from the nanowires and copper and carbon come from the TEM grid.

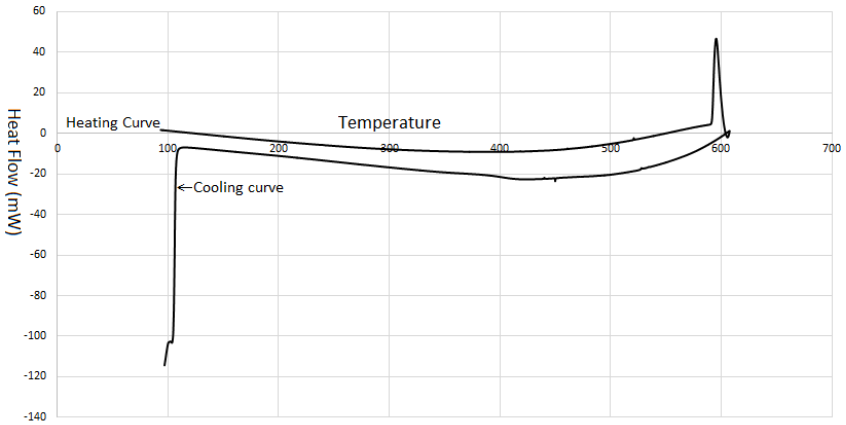

Figure S2: DSC of tungsten oxide sol-gel starting with powders which were heat treated and stabilized at 350 degrees for 8 hours.

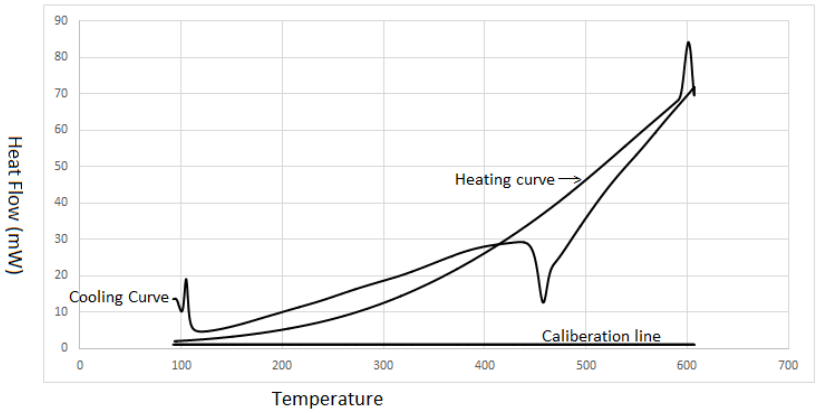

Figure S3: DSC of tungsten oxide sol-gel starting with amorphous (uncalcined) powders.